

A Versatile Hong-Ou-Mandel Interference Experiment in Optical Fiber for the Undergraduate Laboratory

Cyrus Bjurlin and Theresa Chmiel

University of Minnesota, School of Physics and Astronomy, Minneapolis, Minnesota

(Dated: April 1, 2024)

Abstract

Hong-Ou-Mandel (HOM) interference is a quantum optics laboratory experiment that has recently become more accessible to undergraduate students. The experiment consists of two identical photons simultaneously entering a non-polarizing beam splitter. The wavefunctions destructively interfere and the photon pairs bunch at the outputs whereas classically they are equally likely to exit different outputs. Due to the precision needed to achieve indistinguishability, setup and alignment of this experiment is often considered to be too difficult and time consuming to be appropriate for an undergraduate lab, with an end goal of merely demonstrating the HOM interference dip. Here, we present an alternative optical fiber-based apparatus that gives a consistently reproducible experiment with interference occurring in a fused-fiber coupler instead of a traditional beam splitter. We use a commercially available fiber coupled biphoton source that requires minimal alignment and increases coherence length of the interference. In addition, our biphoton source provides direct temperature based control of the frequency degeneracy of the photon pairs produced, allowing for students to investigate physical properties of HOM interference such as coherence length and interference visibility. Through use of standard opto-mechanical parts combined with the commercially available fiber integrated biphoton source and laser, our apparatus is a middle ground between built-from-scratch and pre-aligned setups.

I. INTRODUCTION

The nature of interference at the quantum scale is a source of confusion for many physics students. One such phenomenon is known as Hong-Ou-Mandel (HOM) interference and was first demonstrated by Hong et al. in 1987.¹ HOM interference consists of two individual photons entering the two input ports of a 50:50 non-polarizing beam splitter. When two photons have identical frequency, polarization, arrival time, and position in space, we say they are quantum mechanically indistinguishable, or degenerate. When photons entering the beam splitter are degenerate, the wavefunction destructively interferes. Classically, you would expect to see the two photons exiting at each of the two output ports 50 percent of the time. When interference happens, the photons are more likely to exit the same output port and few to no coincidences are measured. When this happens, we say that photons "bunch" at the output. This makes HOM interference a very intuitive demonstration of quantum optics.

HOM interference is realizable in an undergraduate laboratory,²⁻⁴ however it is usually implemented as a demonstration. The reason for this is that alignment of an HOM apparatus can be difficult and time consuming for an undergraduate student to perform. In order to achieve indistinguishable photons, the two input beams of the beam splitter must be aligned horizontally and vertically so that they intersect at the center of the beam splitter and the two photons must enter the beam splitter almost simultaneously. Furthermore, the common method of producing photon pairs using spontaneous parametric down conversion in β -Barium Borate crystals produces photon pairs that have an HOM coherence length on the order of 10 microns,^{1,3} which is a level of precision that often requires tedious alignment steps at the beam splitter before aligning the actual interference beams. Due to these many limitations, investigating anything more than initial interference would be too intensive a project for most undergraduate teaching labs to find worthwhile.

We address these challenges by presenting an apparatus that not only allows for easier alignment, but also provides opportunities to investigate other physical properties of HOM interference. Through the use of both commercially available pre-aligned parts as well as parts that must be aligned by the student, we find a middle ground between buying a full setup off the shelf and having to meticulously align every part of the apparatus. First, the majority of the apparatus consists of fiber optic cables which minimizes the alignment

procedures necessary. Second, we employ a fiber integrated PPKTP photon pair source that produces pairs with coherence length in the hundreds of microns, making effective simultaneity easier to achieve as well as eliminating the alignment issues that come with in air down conversion. Third, the photon pair source can be tuned to adjust the difference in frequency between the two photons produced as well as the rates of photon pair production. This gives more experimental parameters that can be investigated in relation to the behavior of HOM interference. The remainder of the apparatus however must be built and aligned by the student giving them valuable experience with opto-mechanical setup. The combination of commercially available and do-it-yourself parts makes this apparatus ideal for a longer advanced undergraduate experiment as it can't be completed in a week, but it isn't so difficult that a student couldn't achieve it.

II. APPARATUS

The interfering photon pairs are produced using a phenomenon known as spontaneous parametric down conversion (SPDC). SPDC occurs when a high-power pump laser hits a crystal with nonlinear optical properties. Pump photons are converted into two photons known as the signal and idler, with the requirement that $\omega_i + \omega_s = \omega_p$ where $\omega_{i,s,p}$ are the frequencies of the idler, signal, and pump respectively. Because the signal and idler are produced at the same time, when we measure photon counts over a sufficiently short time we can assume that if we measure one count at each of two outputs, one is the signal and one is the idler so we have a coincidence. We produce photon pairs using collinear type II SPDC, meaning the signal and idler are polarized orthogonally and emitted in the same direction of travel as the pump photon. Specifically, the nonlinear crystal used is periodically poled potassium titanyl phosphate (PPKTP).⁵

A diagram of the full apparatus is given in Fig 1. The pump laser (Ondax, LMFC-405) is a 405 nm laser diode coupled to single-mode polarization maintaining (PM) fiber. All of the fiber used in the interference apparatus is single-mode and polarization maintaining in order to prevent modal and polarization dispersion⁶. The biphoton source (Qubitek, QES2.2) is coupled to single-mode PM fiber and is directly connected to the pump laser via a ferrule connector/physical contact (FC/PC) fiber mating sleeve (ThorLabs, ADAFC2). This biphoton source consists of a temperature controlled PPKTP crystal with a spectral

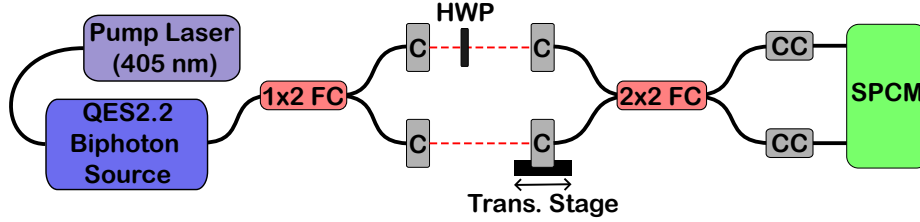


FIG. 1. A diagram of the interference apparatus. 1x2 FC is the one input two output fused-fiber coupler, C labels the 810 nm collimators, HWP is the 810 nm half-wave plate, 2x2 FC is the two input two output fused-fiber coupler, CC labels the coupler cages which filter visible light, and SPCM stands for single photon counting module which records both single photon and coincidence rates for the two fiber coupler outputs. The solid connecting lines in the diagram are single mode polarization maintaining fiber optic cable and the dotted line is the path of the photons in air.

filter to remove the pump beam from the output. The photon pairs produced then have wavelengths close to 810 nm, with wavelengths of exactly 810 nm for degenerate output. The serial emulator Termite⁷ is used to interface with the biphoton source and control the PPKTP crystal temperature. Due to temperature dependence of PPKTP's optical properties,⁵ the temperature control in the biphoton source allows direct control of the frequency degeneracy of the output. The photon pairs are orthogonally polarized when they leave the biphoton source, where they enter a one input two output fused-fiber coupler (Thorlabs, pfc780f)—labeled 1x2 FC in Fig 1—which separates them between two outputs based on their polarization.

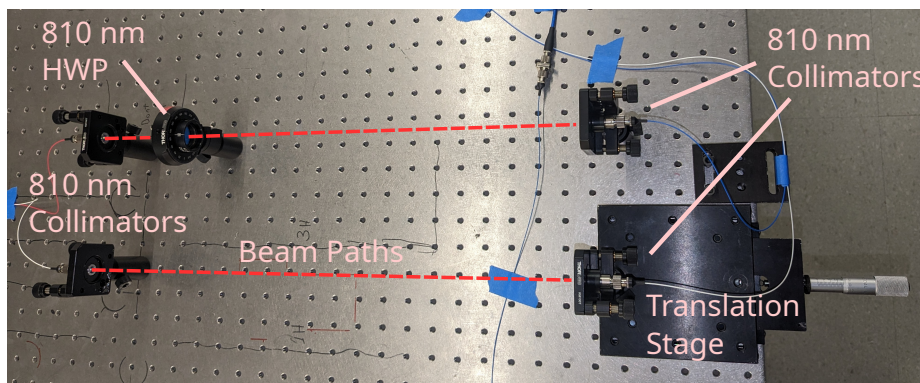


FIG. 2. A labeled picture of the fixed and adjustable delay lines with the beam paths as dashed lines. The 810 nm half wave plate is in the fixed delay line. The translation stage is used to change the length of the adjustable delay line.

The two outputs of the 1x2 coupler are connected using FC/PC connectors to two collimators consisting of a fixed focus collimating lens (Thorlabs, F280FC-780) mounted (Thorlabs, KM100T) with xy tilt control. These two collimators start the in-air section of the apparatus. This section consists of two delay lines, one is fixed and one is adjustable. Details of the two delay lines are shown in Fig 2. Each delay line has another identical collimator at its end. The collimators are all oriented so that the photons leave and enter with vertical polarization and an 810 nm half-wave plate is inserted into the fixed delay line to precisely match the polarization in the adjustable delay line. The adjustable delay line is terminated with a collimator mounted to a translation stage (Parker, 4900 series) which adjusts the optical path-length difference of the photon pair as they enter the next section of the apparatus. The translation stage has a resolution of 0.02 mm and a range of 25 mm which is precise enough to show the shape of the HOM dip but more than large enough to capture the entire dip which is on the order of 1 mm wide.

Because the output of the biphoton source is not visible light, it is easiest to first roughly align the two delay lines using a visible laser and maximizing counts through the delay lines. We use a 633 nm HeNe laser (Melles Griot, 05-lhp-151) which is coupled into a multi-mode fiber (Thorlabs, M31L01) using a collimator with both XY tilt and translation control consisting of a mount (Thorlabs, K6XS) and fixed focus collimating lens (Thorlabs, F220FC-B). More precise alignment is then done using the 810 nm photons.

The collimators at the end of the delay line are connected to a two input two output fused fiber coupler (Thorlabs, PN780R5F2), which is labeled 2x2 FC in Fig 1. Unlike the first coupler, this one takes the two photons in both polarized vertically and it sends each with equal probability to either of the two outputs. This is the analog of a nonpolarizing beam splitter in other HOM setups. The outputs of the 2x2 coupler are connected to two coupler cages, labeled CC in Fig 1, that use longpass filters (Thorlabs, FGL780) to filter out visible light before the remaining photons are sent to the single photon counting module (Excelitas, SPCM-AQRH-13-FC), abbreviated to SPCM, which creates a pulse that is sent to the FPGA counting module (Digilent Nexys3 100 MHz system clock) which records both the counts at each output as well as the coincidences between them.

The data collected by the single photon counting module and FPGA counting module is sent to a computer running a Labview program which shows live plots of single photon and coincidence rates. The program records the raw data to a comma separated values (CSV)

file while more detailed analysis is done in Excel or Matlab.

III. THEORY

A. Fused Fiber Coupling

HOM interference was first demonstrated in a non-polarizing beam splitter and even the demonstrations that use fiber optics often use a beam splitter to achieve the actual interference.^{1,2,8} However in this setup, the HOM interference occurs within a fused fiber coupler. It is therefore necessary to understand what exactly a fused-fiber coupler does to a photon at the quantum mechanical level in order to motivate the theory of the HOM effect.

Fused-fiber couplers are traditionally understood as an application of the evanescent electric field phenomenon.⁹ However, it is equivalent to consider the wave-function of a photon in a single-mode fiber. A single-mode fiber consists of a core several nanometers across surrounded by a cladding of lower refractive index.⁶ This effectively forms a cylindrical potential well. Due to continuity requirements, the wave-function extends slightly out of the core of the fiber into the cladding. When the cores of two fibers are brought very close together with only a small amount of cladding between them, the system turns into two potential wells with a thin barrier, where the wave-function of a photon in one well can bleed into the other. If the wave-function remains in this potential, the probability density will oscillate back and forth between the two wells.¹⁰

A fused fiber coupler then consists of two fibers, usually single-mode, which are fused together in the middle to create the potential described above. By adjusting the length of the coupling region, a manufacturer can control the time that the photon remains in this potential and effectively control the probability of finding the photon at either of the outputs. The fiber coupler is symmetric, so the the probability of staying or switching fibers is the same for both inputs. From a quantum mechanical perspective, the action of a fused-fiber coupler on an input state is the same as the action of a beam-splitter on an input state.⁸ Therefore, just as with a beam-splitter, we can represent the action of the fused-fiber coupler with the unitary 2x2 matrix operator

$$\hat{M} = \begin{pmatrix} t & r \\ -r & t \end{pmatrix} \tag{1}$$

where t is the transmission coefficient and r is the reflection coefficient such that $t^2 + r^2 = 1$. The negative sign on the bottom left r is added to represent a phase change that is required due to energy conservation.¹¹

B. HOM interference

Although our experiment occurs in a fused-fiber coupler, it is instructive to consider exactly what HOM interference is in a beamsplitter before considering a more mathematically rigorous treatment of the coupler interference. When two photons come to the two inputs of a 50:50 non-polarizing beam splitter, they can behave in one of four ways.

1. One photon transmits and one reflects, leading to both photons exiting one output.
2. The other photon transmits and the first reflects leading to both exiting the other output.
3. Both photons transmit and exit at opposite outputs.
4. Both photons reflect and exit at opposite outputs.

Classically we would expect to see all four options equally often. However, when the photons are indistinguishable, HOM interference causes options 1 and 2 to become much more likely than options 3 and 4 which in turn leads to a decrease in coincidences measured between the two outputs.

In our experiment we use a fused-fiber coupler which, from Eq. 1, behaves similarly to a beam splitter. With the action of the coupler defined, the purely quantum mechanical phenomenon of HOM interference can be described. Similar to the formulation of Weihs et al.,⁸ the state of the two-photon system entering the coupler (Fig 3) is described by the double integral

$$|\Psi_{in}\rangle = \int \int d\omega' d\omega'' \zeta(\omega', \omega'') |1, \omega'\rangle |2, \omega''\rangle, \quad (2)$$

where

$$\zeta(\omega', \omega'') \propto \delta(\omega' + \omega'' - \omega_p) f_{\omega'_c}(\omega') f_{\omega''_c}(\omega''). \quad (3)$$

Here, $|1, \omega'\rangle$ represents a photon of frequency ω' entering the coupler at input 1, $f_{\omega'_c}(\omega')$ is the single photon frequency distribution, and δ is the Dirac delta distribution, added to

adhere to the constraint that $\omega' + \omega''$ is equal to the pump frequency ω_p . $f_{\omega'_c}(\omega')$ is assumed to be a sharply peaked gaussian distribution with center frequency ω'_c .

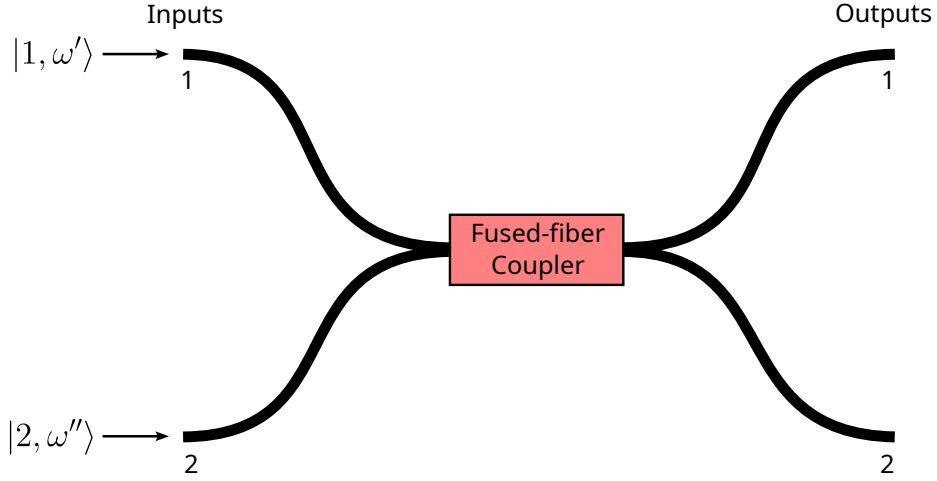


FIG. 3. The two-photon state enters the fused-fiber coupler. Here a photon of frequency ω' enters at input 1 and a photon of frequency ω'' enters at input 2. The fused-fiber coupler then sends photon 1 to outputs 1 or 2 with probabilities t^2 or r^2 respectively and sends photon 2 to outputs 1 or 2 with probabilities r^2 or t^2 respectively.

The interference is then given by the action of the matrix operator \hat{M} on the photons at the two inputs:

$$|\Psi_{out}\rangle = (\hat{M} \otimes \hat{M}) |\Psi_{in}\rangle. \quad (4)$$

Using the final state $|\Psi_{out}\rangle$, the probabilities of finding photons at the outputs can be calculated. The details of these calculations can be found in Campos et al.¹² and produce the probabilities

$$P_{out}(2, 0) = P_{out}(0, 2) = t^2 r^2 [1 + \Phi] \quad (5)$$

$$P_{out}(1, 1) = t^4 + r^4 - 2t^2 r^2 \Phi \quad (6)$$

where

$$\Phi = \int \int \zeta(\omega', \omega'') \zeta^*(\omega'', \omega') d\omega' d\omega''. \quad (7)$$

When the single photon distributions are gaussian as in our case, Φ is evaluated as¹²

$$\Phi = e^{-\frac{\omega_d^2 t_c^2}{8}} \times e^{-\frac{-2\Delta x^2}{c^2 t_c^2}}, \quad (8)$$

where c is the speed of light, $\omega_d = |\omega'_c - \omega''_c|$, t_c is the reciprocal of the spectral width of the two photon distribution, and Δx is the optical path length difference between the photons

arriving at the coupler. This equation assumes the photons to be identical in polarization. When both $\omega_d = 0$ and $\Delta x = 0$, the photons are quantum mechanically indistinguishable and $P_{out}(1, 1) = (t^2 - r^2)^2$ achieves full destructive interference when $t^2 = r^2 = 1/2$. Plotting $P_{out}(1, 1)$ vs Δx gives the characteristic ‘‘HOM dip’’, an example of which is shown in Fig 5, which has a full width at half-maximum given by

$$FWHM_{dip} = ct_c\sqrt{2\ln 2} = l_c\sqrt{2\ln 2} \quad (9)$$

where $l_c = ct_c$ is the coherence length of the two-photon distribution. The FWHM then has an inherent linear correlation to the coherence length of the photon distribution.

C. Dip Width and Temperature

We produce our photon pairs through collinear type II spontaneous parametric down conversion (SPDC).¹³ This specific type of down conversion is highly temperature dependent with slight changes in the temperature of the down converting crystal affecting ω_d for the photon pairs produced.¹⁴ A unique aspect of this experimental setup is the ability to control the crystal temperature in the bi-photon source. In order to understand this relationship, we can investigate the theory for very small changes in temperature around $\omega_d = 0$.

We define the degenerate temperature T_c to be the crystal temperature at which the photon pairs have the same wavelength or $\omega_d = 0$. Fluctuations around T_c will induce fluctuations in the width of the photon distribution ω_d . Defining $\Delta T = |T_c - T|$, we can say that $\Delta T \propto \omega_d$.¹⁴ Therefore

$$\omega_d = \alpha\Delta T, \quad (10)$$

where α is a real constant with units $s^{-1}T^{-1}$. We can now find a relationship between t_c , the coherence time of the two-photon distribution, and ω_d . $t_c = 1/\sigma$ where σ is spectral width of the two-photon distribution.¹⁵ For small ω_d , the two-photon distribution can be approximated by a single gaussian distribution with spectral width $\sigma = \sigma_0 + \omega_d$ where σ_0 is the spectral width of a single photon distribution and also the spectral width of the two-photon distribution when the two photons are degenerate (Fig 4). Here we are assuming that $f'_{\omega'_c} = f''_{\omega'_c}$.¹⁴ Therefore we can write

$$t_c = \frac{1}{\sigma_0 + \omega_d} = \frac{1}{\sigma_0 + \alpha\Delta T}. \quad (11)$$

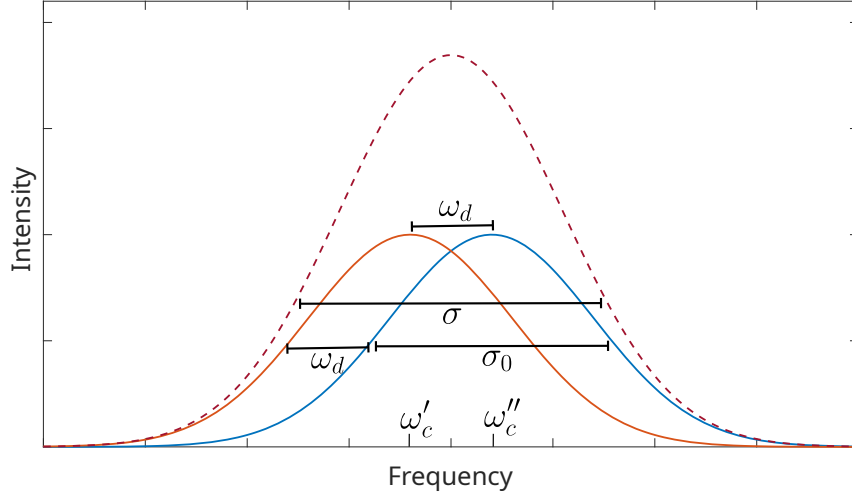


FIG. 4. The two-photon spectrum. The two offset solid curves are the single photon spectra and the dotted line is the combined spectrum. ω_d is the difference between the center frequencies, ω'_c and ω''_c , for each photon. σ_0 is the spectral width for one photon and σ is the spectral width for both photons.

Plugging this into Eq. 9, we find

$$FWHM_{dip} = \frac{\sqrt{2 \log 2} c}{\sigma_0 + \alpha \Delta T} = W_0 \left(\frac{1}{1 + \beta \Delta T} \right), \quad (12)$$

where $\beta = \alpha/\sigma_0$ and W_0 is the FWHM for degenerate photons.

Equation 12 gives an explicit relationship between dip width and crystal temperature. By measuring dip width at various temperatures, we can see the effect that degeneracy has on HOM interference.

D. Treatment of Accidentals

The data collection in this experiment relies heavily on counting coincidences at two detectors. The inherent flaw in doing this is that we can't truly tell when two events are exactly simultaneous. We define a coincidence between two detectors to be when both detectors measure a count within the same time span, called the coincidence window and denoted τ_c . When the gap between individual counts at a detector is much larger than τ_c , this definition of coincidence is very effective at measuring actual instances of simultaneity. However, there will still be some accidental coincidences that don't come from photon pairs.

The rate of accidental coincidences R_{acc} is given by¹⁶

$$R_{acc} = \tau_c R_A R_B \quad (13)$$

where R_A and R_B are the rates measured at detectors A and B respectively. Using this relationship we calculate accidental coincidence rates and subtract them from the overall data.

IV. SAMPLE DATA AND ANALYSIS

In collecting the sample data, coincidence counts and single counts were recorded using a Labview program and analyzed using Matlab. The Labview program records the coincidence rate every 0.3 seconds. For each data point in both Figs. 5 and 6, 60 seconds of coincidence rate data or roughly 200 individual coincidence rates were recorded. The value of each data point is then the average of those coincidence rates. The error bars represent the standard deviation of the mean.

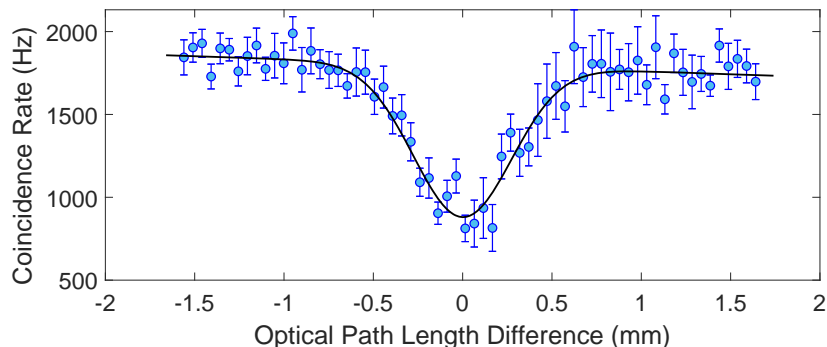


FIG. 5. Coincidence counts plotted against optical path length difference (OPD). Error bars correspond to standard error of the averaged data. Accidental coincidence rates are subtracted and the data is fitted to an inverted gaussian distribution with a linear offset term to account for slight changes in calibration as the translation stage moves. This chart shows the characteristic “HOM dip”, where full interference occurs when the OPD is equal to 0.

Merely demonstrating the existence of the dip is often the end goal of an undergraduate HOM experiment. An example of that result is shown in Fig. 5. Coincidence rates are measured every 0.002 in or 0.0508 mm as the translation stage scans across the point of zero optical path length difference. After the accidental coincidence rates are subtracted out, the

data is fitted to an inverted gaussian distribution with a linear offset. We add the linear offset to the fit because moving the translation stage slightly mis-aligns the adjustable delay line which results in a linear decrease of counts as translation continues.

The depth of the dip, also known as the interference visibility, does not reach zero as would be expected for perfect indistinguishability. The main reason for this is not that the photons aren't indistinguishable but that the two input two output fused-fiber coupler where the interference occurs does not have equal probability of sending a photon to either output. It can be shown using Eq. 6 that the visibility of the dip is given by

$$V = \frac{2r^2t^2}{r^4 + t^4} \quad (14)$$

where t^2 and r^2 are the transmission and reflection probabilities respectively. $V = 0$ when there is no dip and $V = 1$ when the dip goes fully to zero coincidences. In this setup, the fused-fiber coupler is rated to be 50:50 at 780 nm wavelength while interference occurs at 810 nm wavelength. We measured the transmission and reflection of the fused-fiber coupler for degenerate photons and found that $t^2 = 0.329 \pm 0.002$ and $r^2 = 0.671 \pm 0.004$. Using Eq. 14, the maximum visibility that could be recorded using this apparatus is 0.790 ± 0.006 . The data of Fig. 5 does not quite reach this mark, but the remaining difference in visibility could likely be eliminated with more precise polarization matching between the two delay lines.

We demonstrate interference and confirm that the data follows an inverted gaussian model in Fig. 5. This is interesting on its own, but we can investigate more characteristics of HOM interference.

By repeating the measurement process of Fig. 5 for multiple scenarios, we can investigate how degeneracy effects the HOM dip. Because of the temperature control in the QES2.2 biphoton source, we are able to take measurements at non-degenerate wavelengths, altering the width over which destructive interference occurs. In Fig. 6, coincidence rates vs optical path length difference is plotted for five different temperatures near the degenerate temperature T_c . For these graphs, data points were taken every 0.20 mm.

The dip is widest at the biphoton source default temperature T_c , although the difference in widths is small (Fig. 6). This implies that the longest coherence length occurs for frequency degenerate photons, as was predicted. There is also some variation in visibility which we did not investigate theoretically. This data shows the uniqueness of this apparatus;

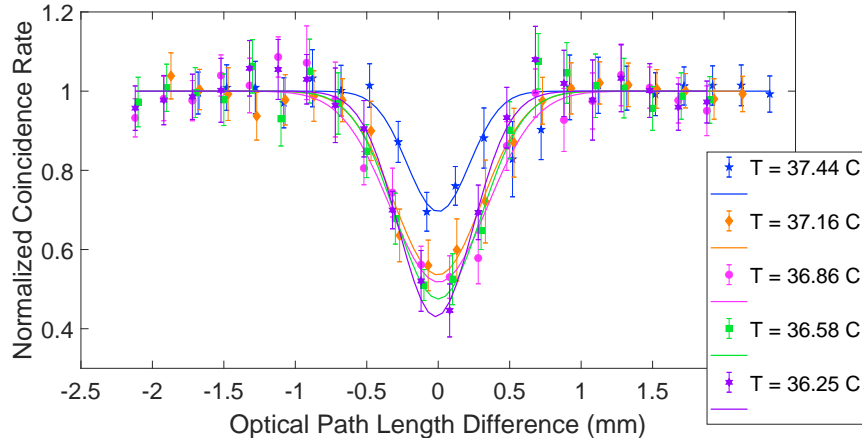


FIG. 6. Coincidence counts plotted against optical path length difference (OPD) for five different crystal temperatures. The data sets are each fitted to an inverted gaussian distribution (Fig. 5) and are normalized with respect to the average coincidence counts outside of the dip with accidentals removed.

measurements for different degeneracies would not be possible for most implementations of HOM interference in an undergraduate lab.^{2,3}

For a more precise investigation of the relationship between degeneracy and coherence length, data is shown at five additional temperatures and the FWHM of the dips is plotted against PPKTP crystal temperature in Fig. 7. The coherence length, l_c , is proportional to the FWHM as shown in Eq. 9. According to this relationship, a second Y-axis is included in Fig. 7 to show coherence length.

This data in Fig. 7 is fitted to a model matching that of Eq. 12. The fit for the data was found to have a reduced Chi-squared value of 0.804 indicating the model is a good match for the data. The data in Fig. 7 exemplifies the utility and uniqueness of this apparatus as temperature control is not often found in undergraduate HOM labs. From the fitting data the maximum FWHM and the central temperature are calculated. T_c is found to be $(36.80 \pm 0.05)^\circ\text{C}$ and W_0 is found to be (0.86 ± 0.05) mm. This value matches the 1 mm expected FWHM quoted by Qubitek.

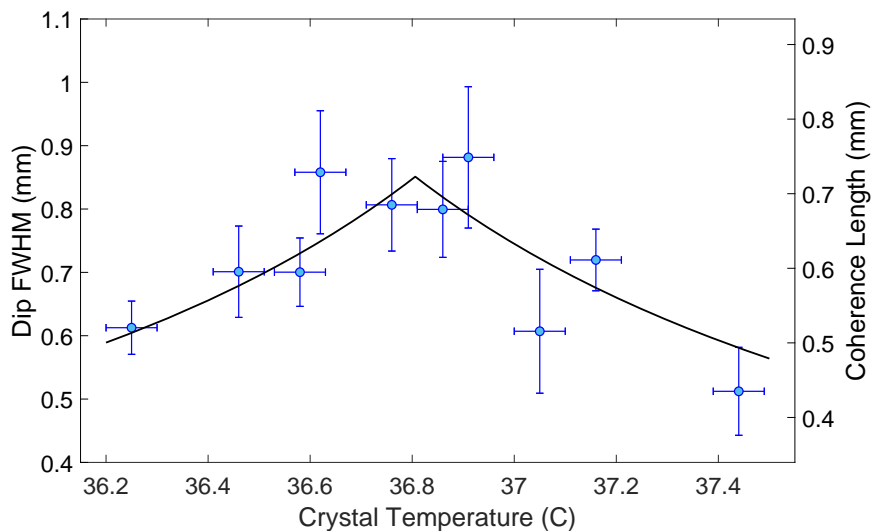


FIG. 7. Dip full width half maximum plotted against PPKTP crystal temperature. This data is assumed to take the form of Eq. 12 and is fitted to a model of that form. Horizontal error bars represent estimated crystal temperature fluctuations, vertical error bars represent a 67% confidence interval in dip width. A second y-axis is added to for coherence length values extrapolated from dip FWHM.

V. CONCLUSION

We presented a versatile and user-friendly apparatus for investigating HOM interference in an undergraduate laboratory. The optical fiber-based apparatus allows for easier investigation of coherence length and interference visibility for both degenerate and non-degenerate photon pairs. As an example of the possible experiments that could be done, we showed a relationship between coherence length and PPKTP crystal temperature.

We demonstrate interference and show that the HOM dip follows an inverted gaussian profile (Fig. 5). We also find that coherence length for HOM interference is inversely correlated to SPDC crystal temperature as predicted by our understanding of the relationship between photon pair degeneracy and coherence length.

This apparatus is well suited for implementation in an undergraduate lab. The multitude of fiber optic components make alignment and setup more intuitive and less tedious for a student who may be less comfortable with experimental optics, while the alignment of the in-air delay lines still gives experience using more traditional optomechanical equipment,

making this lab a perfect middle ground between off the shelf setups and setups built from the ground up. Furthermore, the use of fiber optics, specifically the fused fiber couplers, exposes a student to more specialized physical phenomena, as the physics of fiber optics and SPDC are not commonly included in undergraduate curricula.¹⁷

These types of quantum experiments for undergraduates are being implemented by other labs and they can provide valuable intuition for students towards the behavior of quantum mechanics.¹⁸ Although quantum interference phenomena are common examples of the “weirdness” of quantum mechanics,¹⁹ undergraduates rarely get to see the specific physical characteristics of these phenomena. This apparatus provides that opportunity for HOM interference.

Here, we investigate the relationship between temperature and degeneracy, however there are other possible experiments that could be done. Interference visibility, the depth of the HOM dip, is affected by frequency degeneracy as well as the fused fiber coupler ratio as shown in Eq. 8. The visibility degeneracy relationship could be investigated by measuring the visibility at different temperatures. Because the coupler ratio depends on the wavelength, as the degeneracy is changed, the coupler ratio would also change. This would be a very intriguing experiment to consider since degeneracy affects the visibility directly as in Eq. 8 but it also effects the visibility indirectly by changing the coupler ratio $r^2 : t^2$.

Another experiment that could be done involves the polarization of the interfering photons. In this paper we have exclusively scanned over optical path length difference to create the HOM dips. However, it is equally valid to consider differences in polarization between the photon pairs instead of path length.¹² The behavior of the HOM dips with respect to polarization would be interesting to investigate using this apparatus and would require careful consideration of the how the changes in polarization affect the behavior of the polarization maintaining fused-fiber coupler.

VI. AUTHOR DECLARATIONS

A. Conflict of Interest

The authors have no conflict of interest to disclose.

-
- ¹ Chong-Ki Hong, Zhe-Yu Ou, and Leonard Mandel. Measurement of subpicosecond time intervals between two photons by interference. *Physical review letters*, 59(18):2044, 1987.
- ² Nicholas S DiBrita and Enrique J Galvez. An easier-to-align hong–ou–mandel interference demonstration. *American Journal of Physics*, 91(4):307–315, 2023.
- ³ A Ourjountsev, MC Dheur, T Avignon, and L Jacubowicz. Two-photon quantum interference for an undergraduate lab. *European Journal of Physics*, 36(6):065034, 2015.
- ⁴ Jorge Carvioto-Lagos, Gustavo Armendariz, Víctor Velázquez, Enrique López-Moreno, M Grether, and EJ Galvez. The hong–ou–mandel interferometer in the undergraduate laboratory. *European journal of physics*, 33(6):1843, 2012.
- ⁵ Alessandro Fedrizzi, Thomas Herbst, Andreas Poppe, Thomas Jennewein, and Anton Zeilinger. A wavelength-tunable fiber-coupled source of narrowband entangled photons. *Optics Express*, 15(23):15377–15386, 2007.
- ⁶ KS Thyagarajan and Ajoy Ghatak. *Fiber optic essentials*. John Wiley & Sons, 2007.
- ⁷ Thiadmer Riemersma. Termite: A simple rs232 terminal, 2019.
- ⁸ Gregor Weihs, Michael Reck, Harald Weinfurter, and Anton Zeilinger. Two-photon interference in optical fiber multiports. *Physical Review A*, 54(1):893, 1996.
- ⁹ Bishnu Pal. Fabrication and modeling of fused biconical tapered fiber couplers. *Fiber and integrated optics*, 22(2):97–117, 2003.
- ¹⁰ Enrique Peacock-López. Exact solutions of the quantum double square well potential. *Chem. Educator*, 11:383–393, 2006.
- ¹¹ Dmitry Makarov. Theory for the beam splitter in quantum optics: Quantum entanglement of photons and their statistics, hom effect. *Mathematics*, 10(24):4794, 2022.
- ¹² Richard A Campos, Bahaa EA Saleh, and Malvin C Teich. Fourth-order interference of joint single-photon wave packets in lossless optical systems. *Physical Review A*, 42(7):4127, 1990.
- ¹³ Qubitekk. Quantum mechanics education and research. <https://www.compadre.org/advlabs/bfyiii/files/QubitekkBrochureDigital05122017final.pdf>, 2017.
- ¹⁴ Fabian Steinlechner, Marta Gilaberte, Marc Jofre, Thomas Scheidl, Juan P Torres, Valerio Pruneri, and Rupert Ursin. Efficient heralding of polarization-entangled photons from type-0

- and type-ii spontaneous parametric downconversion in periodically poled ktiopo 4. *JOSA B*, 31(9):2068–2076, 2014.
- ¹⁵ Yu Yang, Luping Xu, and Vittorio Giovannetti. two-parameter hong-ou-mandel dip. *Scientific Reports*, 9(1):10821, 2019.
- ¹⁶ Brett J Pearson and David P Jackson. A hands-on introduction to single photons and quantum mechanics for undergraduates. *American Journal of Physics*, 78(5):471–484, 2010.
- ¹⁷ National Research Council et al. Adapting to a changing world: Challenges and opportunities in undergraduate physics education. 2013.
- ¹⁸ Enrique J Galvez. Resource letter spe-1: Single-photon experiments in the undergraduate laboratory. *American Journal of Physics*, 82(11):1018–1028, 2014.
- ¹⁹ William J Mullin. *Quantum weirdness*. Oxford University Press, 2017.